2025 26th International Conference on Thermal, Mechanical and Multi-Physics Simulation and Experiments in Microelectronics and Microsystems (EuroSimE) | 979-8-3503-9300-2/25/$31.00 ©2025 IEEE | DOI: 10.1109/EUROSIME65125.2025.11006563

# Modeling and Lumped-element Extraction of PCB-based Laterally Coupled Coplanar Transformers

Ozberk Ozturk
*Faculty of Engineering and Natural Sciences*
*Sabanci University*
Istanbul, Turkiye
ozberk@sabanciuniv.edu

Najeh Zeidi
*ICTEAM Institute*
*UCLouvain*
Louvain-la-Neuve, Belgium
najeh.zeidi@uclouvain.be

Fares Tounsi
*ICTEAM Institute*
*UCLouvain*
Louvain-la-Neuve, Belgium
fares.tounsi@uclouvain.be

Denis Flandre
*ICTEAM Institute*
*UCLouvain*
Louvain-la-Neuve, Belgium
denis.flandre@uclouvain.be

Murat Kaya Yapici
*Faculty of Engineering and Natural Sciences*
*Sabanci University,* Istanbul, Türkiye
*Department of Electrical and Computer Engineering University of Washington*, Seattle, USA
murat.yapici@sabanciuniv.edu

***Abstract*—In this paper, we present a comprehensive analysis of concentric and interleaved coplanar transformer models, focusing on key performance parameters such as self-inductance, resistance, mutual inductance, and interwinding capacitance. These parameters are used to develop a lumped-element model that accurately represents the behavior of a coplanar transformer. We propose a universal method based on FEM simulations to extract each parameter value, while the validity of the lumped model is verified by comparisons with measurements obtained from printed circuit board (PCB) transformers and HFSS simulations.**

***Keywords—planar transformers, FEM simulations, mutual inductance, interwinding capacitance.***

## I. Introduction

The growing demand for high-frequency applications requiring compact form factors and high power densities has led to significant interest in planar transformer designs in recent years [1, 2]. Planar transformers can be seamlessly integrated into printed circuit boards (PCBs), making them ideal for high-frequency power conversion applications. Additionally, they offer several advantages over traditional wire-wound transformers, including improved thermal performance, high power density, repeatability, and low leakage inductance. Among planar transformer topologies, there are three basic classifications: stacked, interleaved, and concentric [3, 4]. These terms describe the relative spatial arrangement of the windings with respect to each other in three dimensions.

In stacked transformers, the primary and secondary windings are arranged in distinct, vertically stacked layers, separated by an insulating layer. In this configuration, magnetic coupling and mutual inductance between the windings are maximized since the vertically stacked metal layers share the same surface area. As a result, traditional designs often feature windings with identical layouts in each layer. This configuration has the highest interwinding capacitance between windings because it relies on complete overlap between layers and is therefore more suitable for low-frequency/high-isolation systems.

In the interleaved transformer topology, the primary and secondary windings are alternately arranged side-by-side on a single planar layer in order to improve magnetic coupling and reduce leakage inductance [5, 6]. This means that each turn of the secondary winding is between consecutive turns of the primary winding, and vice versa. In this topology, the magnetic coupling occurs laterally (within the same layer) rather than vertically (across layers), resulting in moderate coupling compared to stacked transformers and reduced interwinding capacitance due to lateral coupling between adjacent traces. This topology is more suitable for high-frequency applications (e.g., MHz-range converters) and low-power converters (e.g., wearables, IoT).

Similarly, concentric (or tapped) transformers are designed with both primary and secondary windings arranged radially on the same plane [7]. In this configuration, the primary encircles the secondary or vice versa, creating an arrangement where the windings are nested as inner and outer spirals. This design allows for higher self-inductances and lower interwinding capacitances, while the inductive coupling factor ($k$) is generally limited. The interwinding capacitance, which appears between the overlapping radial segments of the primary and secondary windings, is moderate due to the proximity of adjacent turns [8]. This topology is a balanced compromise between magnetic coupling and interwinding capacitance, making it suitable for RF/wireless applications (e.g., NFC, resonant charging) where symmetry is essential.

The ease and popularity of multilayer PCBs, where 12 layers are accessible even to electronics hobbyists, has contributed to the use of stacked transformers. The repeated distribution of the same pattern in each layer allows analysis of the magnetomotive force over the entire geometry in the normal direction, effectively simplifying the problem into a one-dimensional (1D) study [1]. In contrast, the concepts of interleaved and concentric transformers, placing both coils in the same plane, make the analysis of the magnetic coupling of the circuit two-dimensional (2D) and more complex. Although there is abundant literature on the 1D magnetomotive force analysis of transformers, the 2D cases where the primary and secondary windings are placed together on the same plane have not been thoroughly investigated to date [9]. The study of such small coplanar transducers may be relevant for radio frequency devices, wireless power transmission, or sensing applications. It is therefore the motivation of this paper to focus on the analysis of coplanar

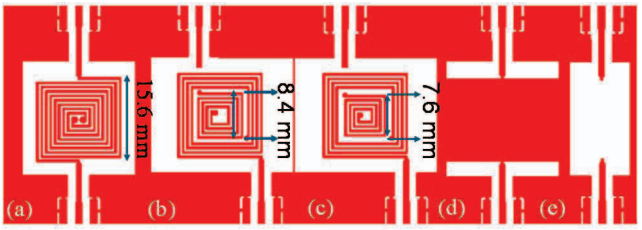


Fig. 1. Three coplanar transformer designs: (a) interleaved design $T_1$; (b) concentric design $T_2$; (c) concentric design $T_3$. Together with (d) short and (e) open de-embedding dummies.

transformers and propose an electromagnetic (EM) simulation-based approach, using ANSYS HFSS, to construct and design the lumped-element model.

Specifically, in this paper, two distinct coplanar transformer topologies (concentric and interleaved) were fabricated on an FR4-based PCB, and their electrical network parameters were extracted. Then, EM simulations were setup with the same geometry and material properties, which demonstrated a close match between the measured and simulated network parameters. Once the validity of the simulations was established for each transformer, test structures specifically designed for lumped element extraction were analyzed in HFSS, and lumped element models were developed.

## II. Manufacturing and Measurements

To study laterally coupled coplanar transformers, three different designs (Fig. 1a-c) with the same footprint (named $T_1$, $T_2$, and $T_3$) were chosen. They include an interleaved transformer ($T_1$ in Fig. 1a) and two concentric transformers with different winding separation distances ($T_2$ and $T_3$, in Fig. 1b and c, respectively). All designs feature a track width of 370 µm and a separation distance of 430 µm between adjacent traces while occupying the same area of 15.6 mm × 15.6 mm. The first concentric design ($T_2$) has a separation distance of 800 µm between its inner and outer windings with an internal inductor diameter of 8.4 mm, while the second concentric design ($T_3$) has a separation distance of 1200 µm with an internal winding diameter of 7.6 mm. In addition, two dummies were designed for open/short de-embedding: the first structure shorted the coplanar waveguide between the two ports, and the second completely removed the metal between the two ports, leaving them unconnected (Fig. 1d-e).

All three transformers were fabricated on a double-side FR4 board with 35 µm-thick gold-plated copper traces ($\sigma = 5.15\text{x}10^7$ S/m) on each side and a relative permittivity of $\varepsilon_r = 4.7$ (Fig. 2). The devices were characterized using a Keysight E5080A vector network analyzer (VNA) over a frequency range of 100 kHz to 3 GHz. Prior to the measurement, the effects of wiring and connector transitions were eliminated from the VNA using the "short-open" calibration (SOC) method, which shifted the measurement reference plane to the SMA connector on the PCB. Following the VNA measurements, the reference plane was further advanced towards the coplanar transformers using the open-short (dummies in Fig. 1d and e) de-embedding method. This process isolates the influence of the waveguide and the surrounding ground plane from the measurements. During de-embedding, the S-parameters of the measurements are

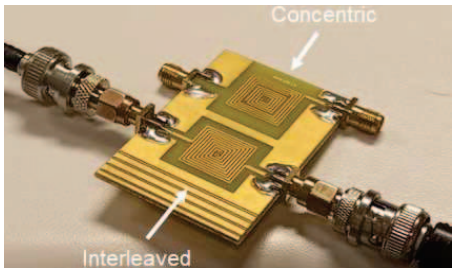


Fig. 2. VNA measurement of interleaved $T_1$ and concentric $T_2$ transformers fabricated on PCB.

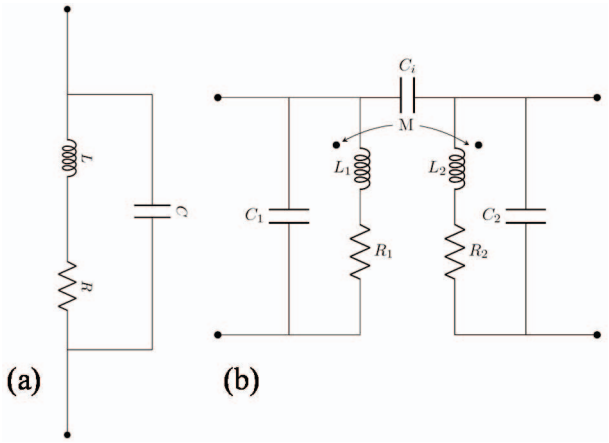


Fig. 3. Lumped-element model on PCB for the (a) planar inductor, and (b) planar transformer.

converted into admittance and impedance parameters of the transformers ($Y_{DUT}$) and the open and short dummies ($Y_{open}$ and $Y_{short}$).

Hence, the Y-parameters of the de-embedded coplanar transformers ($Y_{cp}$) can be extracted according to [10]:

$$Y_{cp} = \left[ \left( Y_{DUT} - Y_{open} \right)^{-1} - \left( Y_{short} - Y_{open} \right)^{-1} \right]^{-1} \quad (1)$$

This last equation removes parasitic capacitances and connections from the measurement, and its effect can be directly observable on the impedance parameters, as the resonant frequency then shifts to higher frequencies.

## III. Extraction Methodology

The lumped-element model of a single planar inductor on a PCB can be represented as an RLC network (Fig. 3a) [11]. This model includes a self-inductance $L$, a series resistance $R$ to account for the dissipative effects on the metal traces, and a parallel capacitor $C$ to incorporate the capacitive coupling arising from the interaction between adjacent traces between turns of the spiral. The case of a planar transformer can be understood by extending the model to include a mutually coupled secondary inductor. The overall model is illustrated in Fig. 3b, where the same RLC branches describe both planar inductors while also incorporating the mutual inductance $M$ and the interwinding capacitance $C_i$ terms to account for the interaction between the two windings [11].

In each planar transformer, the RLC parameters of each winding ($L_{1,2}$, $R_{1,2}$, and $C_{1,2}$) can be extracted separately. Among the formulas in the bibliography, some are well-established parametric formulas for self-inductance and resistance calculations, while others are more complex empirical calculations. For self-inductance calculations of the

planar spiral inductors, the modified Wheeler formula can be used [12]:

$$L_{mw} = K_1 \mu_0 \frac{n^2 \, d_{avg}}{1 + K_2 \, p} \tag{2}$$

where $\mu_0$ is the vacuum magnetic permeability ($4\pi\times10^{-7}$ T m/A), $n$ is the number of turns, $d_{avg}=0.5(d_{out}+d_{in})$ is the average diameter, and $p= (d_{out} \; d_{in})/(d_{out} + d_{in})$ is the fill ratio. The coefficients $K_1$ and $K_2$ in Eq. 2 also include the effect of the spiral layout in the inductor and consider the roundness of the spiral, whether it is rectangular or circular. To calculate the parasitic resistance $R$, each winding can be treated as rectangular metal traces, where the skin-depth $\delta$ also becomes important at high frequencies; the following equation is used [13]:

$$R=\frac{\rho \, l}{w \, \delta \, (1-e^{\frac{-t}{\delta}})} \tag{3}$$

$$\text{with,} \qquad \delta = \sqrt{\frac{2\rho}{2\pi f \mu_0 \mu_r}} \tag{4}$$

where $\rho$ is the resistivity of the conductor material, $w$ and $t$ are the width and the thickness of the trace, and $l$ is the total length of the inductor. These values for a planar inductor can be also extracted using its impedance parameters $Z_{11}$. By analyzing the inductor around its operating frequencies (before resonance), the real part of the impedance parameter provides the resistance, through $R=Re(Z_{11})$, while the imaginary part reveals the reactance, which can be used to determine the inductance, through $L=Im(Z_{11})/2\pi f$. The resonant frequency then allows calculating the capacitance, through $C = \frac{1}{L \, \omega_{res}^2}$, where $\omega_{res}$ is the angular resonant frequency of the inductor. For parameter extraction, electromagnetic (EM) simulations were performed in ANSYS HFSS using the previously mentioned material properties and specific arrangement setups (Fig. 4). The simulations were configured with an adaptive solution setup, including a maximum of 12 passes and a convergence of $\Delta S = 0.002$. A driven modal analysis was used, and solutions were calculated at 500 frequency points logarithmically distributed between 100 kHz and 3 GHz. Open-short de-embedding dummies were also simulated for each transformer to remove the effect of wave ports and transmission lines, thus shifting the reference plane towards the windings. The HFSS simulation setups for the outer inductor and inner inductor parameter extractions are shown in Figs. 4b and 4c, respectively.

For planar transformers, HFSS simulation setups with both primary and secondary windings are used as illustrated in Fig. 4a. The network parameters from the two-port measurements are required for calculating the mutual inductance ($M$) and the coupling coefficient ($k$), as they directly carry the energy transfer information between the windings. These last two parameters can be found by [10]:

$$M = \frac{Im(Z_{12})}{2\pi f_{req}} \tag{5}$$

$$k = \sqrt{\frac{Im(Z_{12}) \; Im(Z_{21})}{Im(Z_{11}) \; Im(Z_{22})}} \tag{6}$$

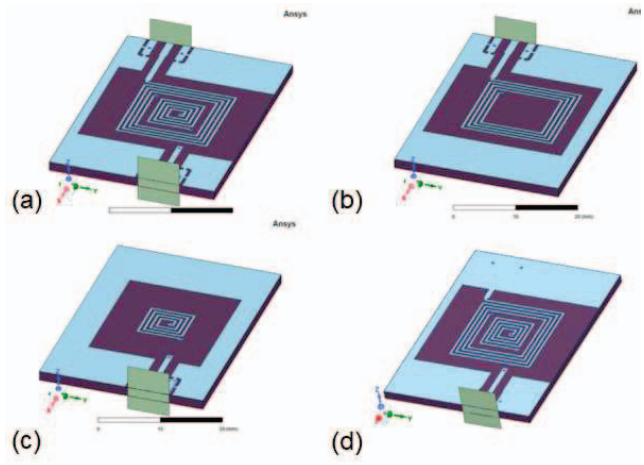


Fig. 4. HFSS simulation setups for the parameter extractions. (a) complete planar transformer; (b) outer inductor only; (c) inner inductor only; (d) inner coil with outer coil grounded.

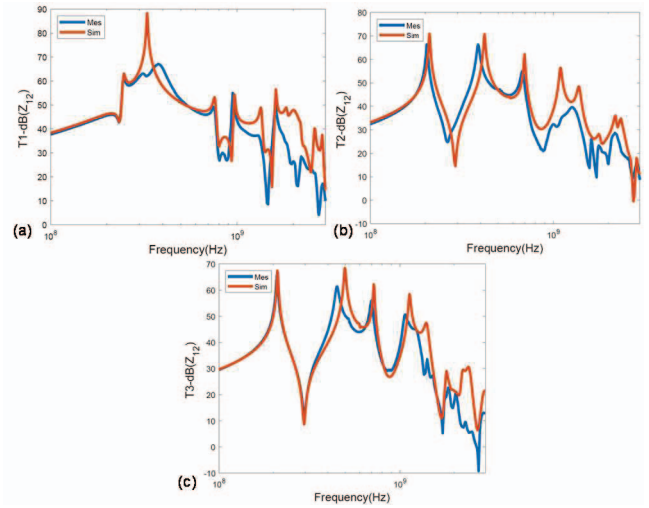


*Fig. 5: Comparison between the $Z_{12}$ parameters of the VNA measurements and simulations for $T_1$, $T_2$, and $T_3$ shown from 1 MHz to3 GHz.*

On the other hand, to calculate the interwinding capacitance, a test structure slightly modifying the transformer is used. In this configuration, the impedance of the 1-port internal inductor (or vice versa) is measured while the external inductor (or vice versa) is still in place but grounded (Fig. 4d). In this configuration, the grounded inductor will be equivalent to a ground point, and the equivalent lumped-element model is given by the RLC circuit of the internal inductor connected in parallel to $C_i$. Therefore, calculating the capacitance differences between this structure and that of the 1-port inner inductor (or vice versa) gives the interwinding capacitance.

## IV. Extraction Results

Comparisons of the impedance parameters ($Z_{12}$) between the VNA measurements and the HFSS simulation over the 100 MHz–3 GHz frequency range of the three transformers are shown in Fig. 5a-c. As can be seen, the simulation results closely match the measurements, indicating a successful simulation setup, with near-perfect overlap up to the resonant frequency. Among the three designs, the third concentric transformer ($T_3$) had the best correlation, followed by the

TABLE 1. LUMPED PARAMETERS EXTRACTED FROM HFSS SIMULATIONS FOR EACH TRANSFORMER TOGETHER WITH THEORETICAL VALUES.

| | $T_1$ | | $T_2$ | | $T_3$ | |
|---|---|---|---|---|---|---|
| | **Sim** | **Theo** | **Sim** | **Theo** | **Sim** | **Theo** |
| **$L_1$ (nH)** | 176 | 182.9 | 372.73 | 384.21 | 372.73 | 384.21 |
| **$R_1$ (Ω)** | 0.305 | 0.22 | 0.306 | 0.298 | 0.306 | 0.298 |
| **$C_1$ (pF)** | 1.18 | - | 1.14 | - | 1.14 | - |
| **$L_2$ (nH)** | 176 | 182.9 | 111.62 | 117.38 | 91.76 | 91.36 |
| **$R_2$ (Ω)** | 0.22 | 0.22 | 0.129 | 0.134 | 0.124 | 0.115 |
| **$C_2$ (pF)** | 1.18 | - | 1.1 | - | 0.77 | - |

For the single inductor R-L values, analytical calculations have been added for comparison purposes.

TABLE 2. LUMPED-ELEMENT PARAMETERS RELATED TO THE COUPLING BETWEEN THE TWO WINDINGS.

| | ***M* (nH)** | ***$C_i$* (pF)** | ***k*** |
|---|---|---|---|
| **$T_1$** | 120.4 | 2.44 (2.85) | 0.659 |
| **$T_2$** | 59.9 | 0.55 (0.43) | 0.277 |
| **$T_3$** | 40.7 | 0.47 (0.36) | 0.222 |

second concentric transformer ($T_2$), and then the interleaved transformer ($T_1$). This is understandable, as the stray capacitance values are higher for $T_1$ and $T_2$ which degrade the measurements.

After validating the simulations against the VNA measurements, the same simulation setups shown in Figs. 4a to 4d were used to extract the parameters for the three transformers. TABLE 1 shows the single coil parameters ($R_i$, $L_i$, and $C_i$, where $i = \{1, 2\}$) extracted from the simulations, while TABLE 2 lists the coupling parameters $M$ and $C_i$. The analytically calculated self-inductance and resistance values were also added for comparison. The flexibility of the FEM simulations allowed rapid trials on different structures for parameter extraction, which was particularly important for calculating interwinding capacitance. It is worth mentioning that the authors had never encountered this solution before in the literature, where the difference between the capacitances shown in Figs. 4d and 4c is used for interwinding capacitance calculations.

Since both windings of the interleaved transformer ($T_1$) are identical, they share the same parameter values. This is also true for the outer (primary) windings of the concentric transformers $T_2$ and $T_3$. The difference between the values was also as expected, with $T_1$ having the highest coupling coefficient and interwinding capacitance while $T_2$ had the best coupling compared to $T_3$ because the distance between the windings is smaller. Besides these parameters, another point of comparison between the transformers is their bandwidth and maximum possible operating frequency. This could be compared with the simultaneous plotting of the mutual inductance curves in Fig. 6 for the three transformers. For the interleaved transformer $T_1$, the M curve was flat up to 210 MHz, while for $T_2$ and $T_3$ the bandwidth was noted up to 140 MHz. Since the bandwidth of concentric transformers is limited by the self-resonant frequency of the outer inductor, $T_2$ and $T_3$ have roughly the same bandwidth. However, transformer $T_1$ had a higher bandwidth than $T_2$ and $T_3$ because the resonant frequency of its windings was higher.

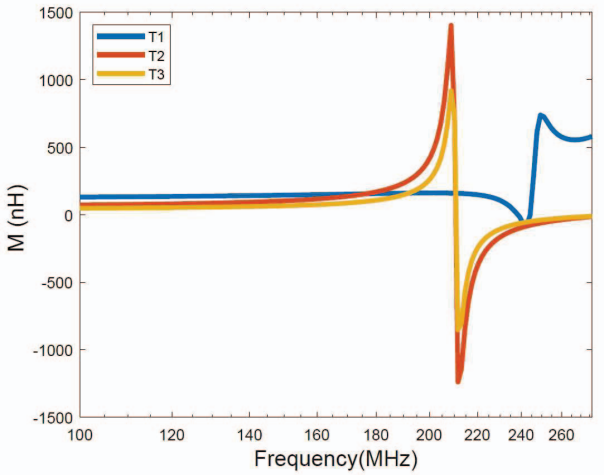


Fig. 6. Mutual inductance for $T_1$, $T_2$, and $T_3$, showing operating bandwidth.

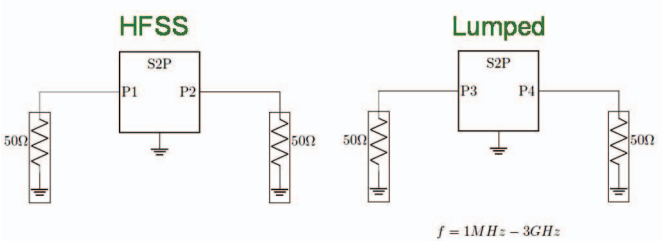


Fig. 7. Impedance parameter comparison between HFSS simulations and the lumped element model

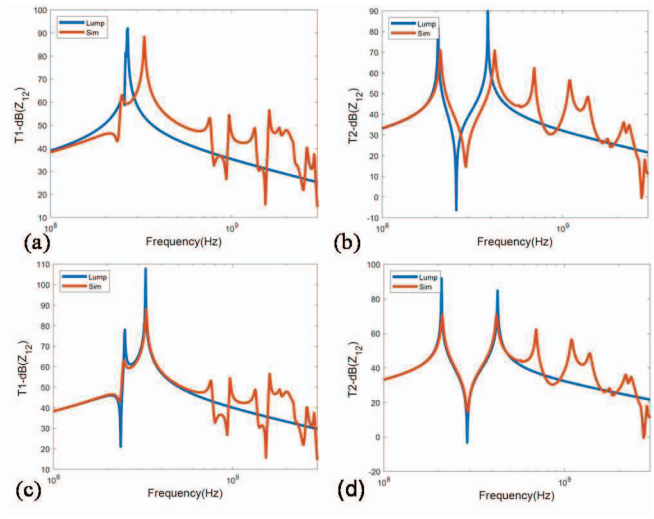


Fig. 8. Comparison of $Z_{12}$ parameter between the constructed lumped-element model and the simulated structure for the transformers $T_1$ and $T_2$; (a-b) comparison before tuning for $T_1$ and $T_2$, and (c-d) presents the results after tuning.

Finally, the accuracy of parameter extraction was tested by building the lumped-element circuits in Keysight ADS. The 2-port network parameters from the lumped-element circuits were calculated and compared with the network parameters from the HFSS simulations (Fig. 7). The impedance parameters from both methods were close, but a visible difference in the capacitance values was observed, particularly high for the interleaved transformer (Fig. 8a, b). These differences were corrected using the parameter tuning mode in ADS (see Fig. 8c, d), as the initial parameters were close to the final values. The corrected capacitance values were shown in parentheses in TABLE 2. As shown in Fig. 8b, the concentric transformer $T_2$ had a smaller tuning error

compared to the interleaved transformer $T_1$; this was expected since the capacitive coupling of interleaved transformers is inherently higher and its variations have a large effect. This also suggests that the parameter extraction method presented here performs slightly better for concentric transformers than for interleaved transformers.

## V. Conclusions

This study focused on extracting performance parameters from coplanar transformers, namely interleaved and concentric configurations. A lumped-element model for transformers was proposed, investigated, and studied with three transformer structures. PCB fabrications and VNA measurements were performed to obtain reference data, which were used to validate the FEM simulations in HFSS. A parameter extraction method based on FEM simulation was developed to isolate lumped elements. This method used three additional simulation structures, in addition to the two-port transformer simulation, including single-coil simulations of the primary, secondary, and secondary with the primary grounded. These latter two structures were used together to determine the interwinding capacitance. After parameter calculations, lumped-element circuits were constructed in ADS, and their accuracy was tested against the network parameters of the simulated transformer. It was found that lumped-element circuits accurately estimate network parameters, especially for concentric transformers. It was found that lumped-element circuits accurately estimate network parameters, especially for concentric transformers. The test structures presented here can be generalized and fabricated on PCBs with the original transformers. This method allows designers to estimate transformer performance parameters as closely as possible early in the design, using vector network analyzer (VNA) measurements after calibration and subsequent de-embedding.

## Acknowledgment

This work was supported by the Scientific and Technological Research Council of Türkiye (TUBITAK) grant number 122E572. Professor Murat Kaya Yapici appreciates the support of the Turkish Academy of Sciences (TUBA) within the framework of the TUBA Outstanding Young Scientist Award Program (GEBIP'21); the Science Academy for the Young Scientist Award Program (BAGEP'23); and Elginkan Vakfi for the Technology Prize'24.

## References

[1] Ouyang, Z., Hurley, W. G. and Andersen, M. A. E., "Improved Analysis and Modeling of Leakage Inductance for Planar Transformers," in IEEE J. Em. Sel. Top. P., vol. 7, no. 4, pp. 2225-2231, Dec. 2019.

[2] S.R. Cove, M. Ordonez, F. Luchino, and J.E. Quaicoe, "Applying response surface methodology to small planar transformer winding design."IEEE Trans. Ind. Electron, vol. 60(2), pp. 483-493, 2012.

[3] S. S. Mohan, C. P. Yue, M. Hershenson, S. S. Wong, and T. H. Lee, "Modeling and characterization of on-chip transformers", International Electron Devices Meeting, 531–534, Dec. 1998.

[4] John R. Long, "Monolithic Transformers for Silicon RF IC Design", IEEE J. Solid-State Circuits, Vol. 35, No. 9, Sep 2000.

[5] E. Frlan, S. Meszaros, M. Cuhaci, and J. Wight, "Computer-aided design of square spiral transformers and inductors", in Proc. IEEE MTT-S, 661–664, June 1989.

[6] R. Wu, N. Liao, X. Fang and J.K.O. Sin, "A Silicon-Embedded Transformer for High-Efficiency, High-Isolation, and Low-Frequency On-Chip Power Transfer", IEEE Trans. on Electron Devices, Vol. 62, No. 1, 220-223, Jan. 2015.

[7] Zhang, J., Ouyang, Z., Duffy, M. C., Andersen, M. A. E. and Hurley, W. G., "Leakage Inductance Calculation for Planar Transformers with a Magnetic Shunt," in IEEE T. Ind. Appl., vol. 50, no. 6, pp. 4107-4112, Nov.-Dec. 2014.

[8] F. Tounsi, B. Mezghani, L. Rufer, S. Mir, and M. Masmoudi, "Electromagnetic modeling of an integrated micromachined inductive microphone," 4th International Conference on Design & Technology of Integrated Systems in Nanoscal Era, April 2009.

[9] F. Tounsi, D. Flandre, L. Rufer, and L.A. Francis, "Performances Evaluation of On-Chip Large-Size-Tapped Transformer for MEMS Applications," IEEE Transactions on Instrumentation and Measurement, vol. 69(9), pp. 7051 - 7060, Sep. 2020.

[10] S. Chouaibi, M.H. Said, D. Nasr, M.B. Ayed, D. Flandre and F. Tounsi "Mutual Inductance Evaluation Between Two Parallel Conductors on a PCB," 30th IEEE International Conference on Electronics, Circuits and Systems (ICECS), Dec. 2023.

[11] Sunderarajan, Sunderesan, M., "The design, modeling and optimization of on-chip inductor and transformer circuits", PhD thesis, Stanford University, 2000.

[12] Mohan, Sunderarajan S., et al. "Simple accurate expressions for planar spiral inductances," IEEE Journal of solid-state circuits, vol. 34(10), pp. 1419-1424, Oct. 1999.

[13] Wheeler, Harold A. "Formulas for the skin effect," Proceedings of the IRE, vol. 30(9), pp. 412-424, 1942.